Field emission of metal nanowires studied by first-principles methods

Choong-Ki Lee[1]**, Bora Lee**[1]**, Jisoon Ihm**[2] **and Seungwu Han**[1,3]

[1] Department of Physics, Ewha Womans University, Seoul 120-750, Korea
[2] Department of Physics and Astronomy, Seoul National University, Seoul 151-742, Korea

E-mail: hansw@ewha.ac.kr

Abstract
We study the field-emission properties of an ultrathin silver nanowire using
first-principles methods. The simulation and analysis of the field emission are
carried out based on density-functional theory using a localized basis
scheme. Through the explicit time evolution of wavefunctions, we obtain the
emission currents and spatial distributions of emitted electrons from a silver
nanowire. In contrast to carbon nanotubes, the localized states are not found.
Instead, pronounced emission currents are observed for s-like extended states
that are free of nodes in a plane normal to the field direction, and the total
emission currents of a silver nanowire are found to be significantly larger
than those of carbon nanotubes. A quantum-mechanical analysis is presented
to explain the observed current enhancement. On the other hand, an ultrathin
gold nanowire gives much smaller emission currents than the silver nanowire
due to a larger work function.

1. Introduction

Metal nanowires, with diameters in the range of 1–100 nm, have been studied widely owing to their unique physical properties as quasi-one-dimensional objects, as well as their potential applications to sensors [1], catalysts [2], nano-scale circuits [3], and nano-mechanical resonators [4]. In particular, there are several merits to using metal nanowires as a field-emission (FE) tip; by using a template with a controlled density of pores [5], one may easily obtain a uniform field-emitter array. Compared to semiconducting nanowires such as ZnO [6] or GaN [7], the metal-nanowire tip would be advantageous in terms of electric conductivity, which significantly lowers the driving voltage of FE. Experimentally, FE tips based on copper [5], tungsten [8], and gold [9] nanowires have been fabricated with appreciable emission performances. In spite of the accumulating experimental data, the theoretical understanding of FE for metal nanowires has not been elaborated much.

The FE of electrons under applied electric fields is a quantum-mechanical phenomenon which can be understood as a tunneling process across the energy barrier between the vacuum and the emitter. At earlier times, Fowler and Nordheim (F–N) employed a simple model to describe FE processes based on one-dimensional schematic potentials and a free-electron approximation [10]. Although the F–N theory has been successful in analyzing the FE of micron-sized metal tips, the theory can be of limited usage when it is applied to nanostructures. To be more specific, the simple square-well potential and the plane-wave approximation are not appropriate for analyzing the FE of nano-sized emitters because the quantum confinement effect in the cross-sectional dimension would significantly influence their emission currents. Furthermore, the F–N theory neglects the phase variation of the wavefunctions on the plane perpendicular to the emission direction. Another limitation arises when describing electron emission from tip-localized states that can be significant in nanomaterials [11]. Therefore, for a more sophisticated description of FE for nanostructures, it is required to consider realistic potentials and wavefunctions. This can be achieved by a first-principles approach, as has been suggested in [12]. In that method, the FE process can be simulated directly using the time-dependent Schrödinger equation. This method has been applied to study the FE characteristics of various carbon-based nanostructures [11, 13–15]. In this work, we apply the method to study FE for silver (Ag) nanowires. We find that the FE characteristics of metal nanowires are significantly

---

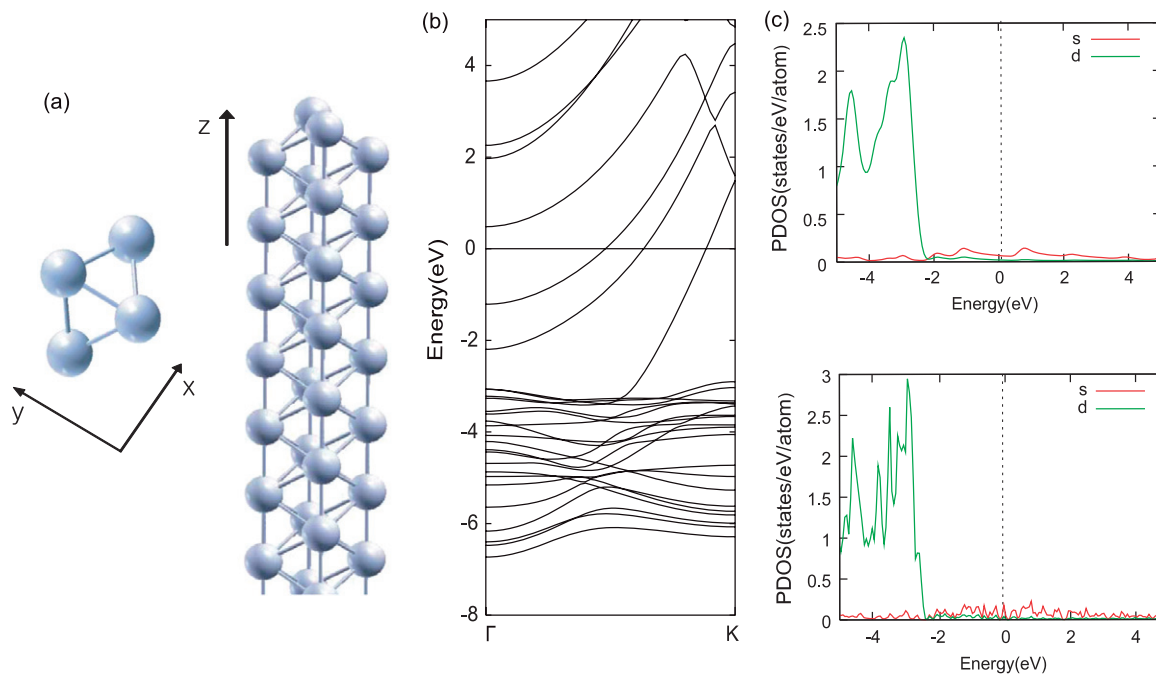[3] Author to whom any correspondence should be addressed.

Figure 1. (a) Top and side views of the atomic structure of the model Ag nanowire. (b) The band structure of an infinite Ag nanowire. The electronic bands at the Fermi level with large dispersions are derived from s-orbitals of Ag atoms. (c) The partial density of states (PDOS) of an infinite nanowire and a finite Ag nanowire with a length of 52 Å are shown in the upper and lower panels, respectively.

(This figure is in colour only in the electronic version)

different from those of carbon nanotubes, and the emission currents are dominated by the extended s-like electronic states of Ag nanowires. The amounts of electronic current under a given condition of local electric field are larger by orders of magnitudes than those of carbon nanotubes.

2. Computational methods

As a model system, we choose ultrathin Ag nanowires with diameters of ∼0.4 nm which were synthesized experimentally [16]. To simulate FE from the nanowire tip, we consider a finite nanowire with a length of 52 Å instead of the semi-infinite model. The electronic states, self-consistent potentials and charge distributions of finite nanowires are obtained by first-principles calculations at the density-functional level using the SIESTA code [17, 18]. We employ the localized basis set with double-ζ polarization to describe the electronic responses accurately. The external electric field is simulated using a saw-tooth-type potential to be compatible with periodic boundary conditions. The local density approximation [19] is used for the exchange–correlation energy of electrons, while the Troullier–Martins-type [20] norm-conserving pseudo-potentials are employed to describe the ion–electron interactions. To obtain the electrostatic potential, a Poisson equation is solved in momentum space using the fast Fourier transform technique, with a grid spacing corresponding to the energy cutoff of 80 Ryd. A supercell of 20 Å × 20 Å × 100 Å is used with vacuum lengths between nanowires bigger than 15 Å. Most multipole interactions between nanowires are negligible at this size of supercell, but the dipole fields

induced by the external field are still substantial and increasing the supercell size results in much larger emission currents. However, this is primarily attributed to a larger local electric field at the emission tip on which the tunneling probability depends exponentially. Therefore, by analyzing the results in terms of the local electric field instead of the external field, one can draw conclusions that are insensitive to the supercell size.

For a description of electron dynamics the electronic wavefunctions of nanowires and self-consistent potentials are expanded by a plane-wave basis set. Due to the incompleteness of the localized basis set, the electronic states obtained from SIESTA are not the exact eigenstates of self-consistent potentials, and therefore they are further relaxed towards true eigenstates through the direct-inversion-in-iterative-space method [21]. The evolution of wavefunctions under the external field is described by the time-dependent Schrödinger equation using the Suzuki–Trotter-type [22, 23] split operator method. The emission current is obtained by monitoring the leakage of electrons from nanowires to the vacuum. For the detailed procedure, we refer readers to [12].

3. Electronic structures of silver nanowire

Figures 1(a) and (b) show the atomic model of an infinite Ag nanowire and its band structure. From the projected density of states (PDOS) in the upper panel of figure 1(c), the electronic bands at the Fermi level are mainly derived from Ag s-orbitals, while most of the d-bands lie below the s-bands. To check any finite-size effect of our model, i.e. an Ag nanowire with a length of 52 Å, the PDOS of finite and infinite Ag nanowires
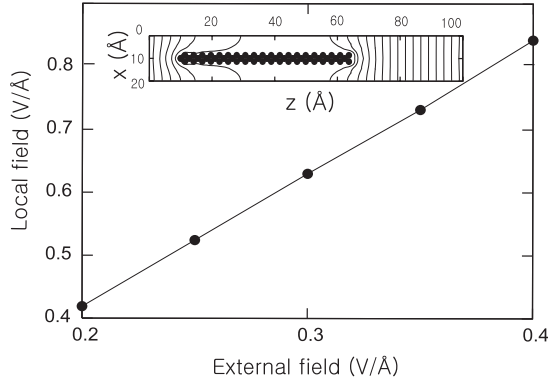
Figure 2. The local electric field measured at the front of an Ag nanowire tip is shown with respect to the external electric field. The inset shows the equipotential lines drawn from the potential difference between $E_{ext} = 0$ V Å^{-1} and $E_{ext} = 0.3$ V Å^{-1}. The contour shape reflects the effect of dipole fields by neighboring cells and the asymmetry along the z-direction is caused by the asymmetric atomic models. The contour spacing is 0.1 Ryd.

are compared in figure 1(c). The overall distributions show good agreement, indicating that the finite model can faithfully reproduce electronic states of the semi-infinite Ag nanowire.

When a saw-tooth-type external electric field of 0.3 V Å^{-1} is applied to the nanowire, the electronic charges are redistributed in a self-consistent manner, and this is reflected in the changes in the electrostatic potentials. The equipotential lines in the inset of figure 2 are drawn from the potential difference between $E_{ext} = 0$ and $E_{ext} = 0.3$ V Å^{-1}. They show that an Ag nanowire can almost perfectly screen the applied electric field, resulting in a sharp enhancement of the electric field at the tip. From the analysis of the charge redistribution, we find that about one electron is accumulated at the tip of the Ag nanowire at the external field of 0.3 Å^{-1}. To estimate the local electric field, we first average the difference in the electrostatic potentials over the xy-plane within 5 Å from the nanowire and then measure the value at 3 Å outside the tip along the z-direction. The results in figure 2 show a nearly

linear relationship between the external field and the local electric field, with a field enhancement factor of 2.1.

4. Emission currents of silver nanowire

As detailed in the above, we obtain the FE current by inspecting the temporal dynamics of the occupied electronic states in the presence of external electric fields. The time interval for the evolution is chosen to be 0.1 au (or 0.002 42 fs) and it is confirmed that the expectation value of a state ($\langle \psi(t)|H|\psi(t)\rangle$, where H is the Hamiltonian and $\psi(t)$ is the wavefunction at time t), is constant within the simulation time. We monitor the time dependence of the charge fraction inside the nanowire, $Q(t)$, and obtain the lifetime, τ, from the time derivative of $Q(t)$. Finally, the current I is obtained from $I = 2e/\tau$. The time dependence of $Q(t)$ in the Ag nanowire is found to be linear until $t = 200$ au and the transition rates are evaluated unambiguously. The emission currents for each energy level are shown in figure 3. The spatial distribution of the wavefunction that gives the largest current is shown as an inset. For comparison, a state close to the Fermi level is also shown. Interestingly, the state without any node in the xy-plane gives the largest current. We recall that the nodal structures in the inset figures are not derived from the orbital characters; states near the Fermi level are mainly derived from s-orbitals. The nodes reflect the phase change between neighboring Ag atoms.

The origin of the large emission current for the nodeless state can be understood in terms of the overlap integral between eigenstates in a nanowire and the vacuum state to which it couples. If the potential variation in the xy-plane is neglected as a first approximation, the electronic wavefunction in vacuum under the applied electric field (z-direction) can be written as $\psi(x, y, z) = e^{i\vec{p}_{\parallel} \cdot \vec{r}/\hbar}\phi(z)$, where $\vec{p}_{\parallel}$ is the transverse component of momentum normal to the emission direction and $\phi(z)$ is a function satisfying the following equation in momentum space:

$$\left[\frac{p_{\parallel}^2}{2m} + \frac{p_z^2}{2m}\right]\phi(p_z) - i\hbar|e|E\frac{d\phi(p_z)}{dp_z} = \varepsilon\phi(p_z), \quad (1)$$
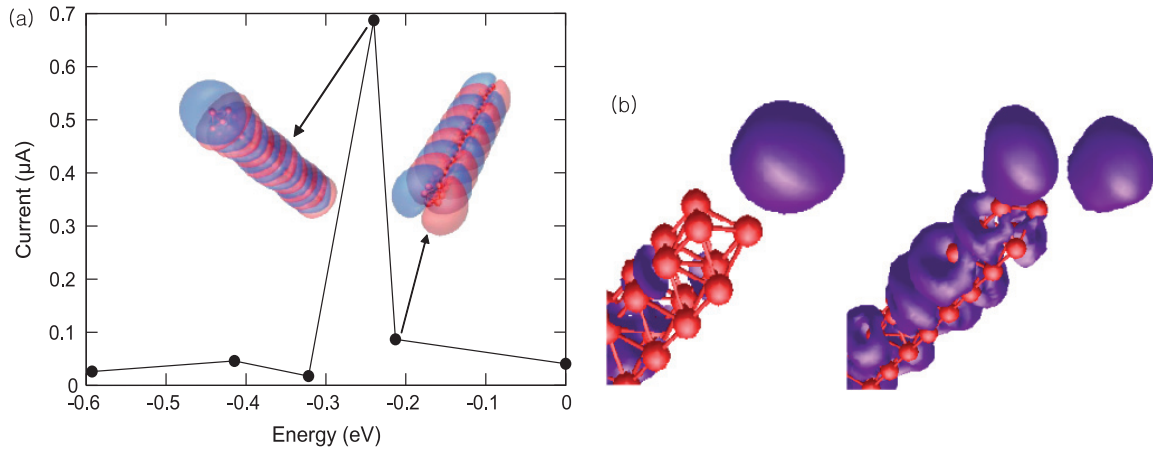

Figure 3. (a) The emission current of an occupied state around the Fermi level, which is set to zero. The external field is 0.3 V Å^{-1}. The inset figures show the spatial distribution of the wavefunctions of representative states. Different shades indicate $+/-$ signs. (b) The isosurface plot for $|\psi(t = 50$ au$)|^2 - |\psi(t = 0$ au$)|^2$ of two states in (a).
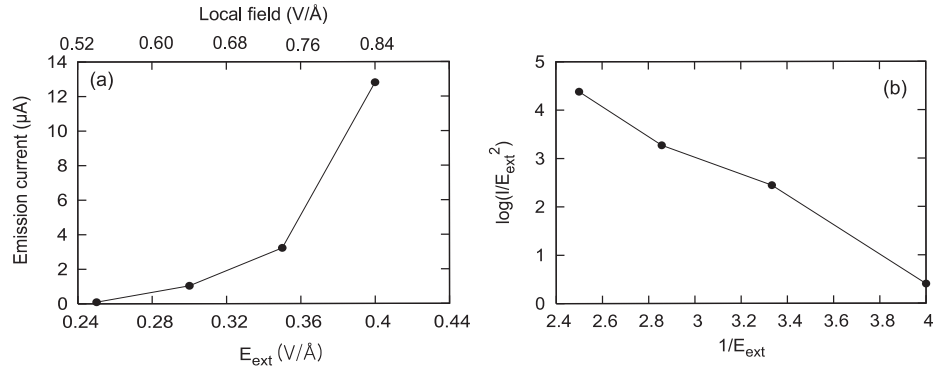
Figure 4. (a) The total emission current of an ultrathin Ag nanowire as a function of the external electric field. The corresponding local electric field is shown in the upper scale. (b) The F–N plot of (a).

where the position operator z is represented as a differential operator in momentum space and E and ε are the local electric field and the energy eigenvalue, respectively. Defining the normal energy, $W = \varepsilon - p_\parallel^2/2m$, the solution of equation (1) can be written in terms of the Airy function, $Ai(x)$;

$$\phi(z) = C\,Ai\left[-(2m|e|E/\hbar^2)^{1/3}\left(z + \frac{W}{|e|E}\right)\right], \quad (2)$$

where C is a normalization constant. On the other hand, the wavefunction in transverse directions can be expanded as follows:

$$e^{i\vec{k}_\parallel \cdot \vec{r}} = A\sum_{n=-\infty}^{n=\infty} i^n J_n\left(\left|\vec{k}_\parallel\right| r\right) e^{in\theta}, \quad (3)$$

where $\vec{k}_\parallel = \vec{p}_\parallel/\hbar$ and $J_n(x)$ is the Bessel function of nth order, (r, θ) are polar coordinates with $\vec{k}_\parallel$ pointing to $\theta = 0$, and A is a constant that does not depend on n. Equation (2) means that the Airy function rigidly shifts toward the nanowire as W increases. Thus, the states with $k_\parallel \sim 0$, i.e. $W \sim \varepsilon$, overlap significantly with electronic states of the nanowire. For small $k_\parallel$, on the other hand, equation (3) indicates that the coefficient for $n = 0$ is the largest ($J_n(0)$ is non-zero only for $n = 0$). Therefore, one can conclude that the state without any node ($n = 0$) in the θ direction, i.e. the s-like state, gives a far larger current than states with a node under the same local electric field.

In a real device, a metal contact is required to maintain steady-state conditions and its impact on the computational results merits discussion. The geometry of the model system (with or without metal electrodes) allows one to separate the wavefunction into xy- and z-components, i.e. $\psi(x, y, z) = \phi(x, y)\xi(z)$. The metallic contact will make $\xi(z)$ complex-valued in the nanowire region with a continuous energy spectrum. On the other hand, the nodal structure in $\phi(x, y)$ is related to the rotational symmetry in the xy-plane and therefore will not be affected by the presence of electrodes. This implies that the pronounced tunneling probability of the nodeless state would be identified in actual devices under steady-state conditions. However, we note that the continuous energy spectrum in the real situation will broaden the sharp peak in figure 3(a) and the current distribution will display a resonance shape centered at the energy of the nodeless states in isolated nanowires. A related question is how the computed

emission currents compare with steady-state currents in a real device. For this, we schematically divide the whole system into three parts—the electrode, nanowire, and vacuum. In analogy with double-barrier tunneling, the steady-state current contributed by a current-carrying mode in a nanowire is given as follows [24]:

$$I = \frac{2e}{\hbar}\frac{\Gamma_1\Gamma_2}{\Gamma_1 + \Gamma_2}, \quad (4)$$

where Γ_1 and Γ_2 (divided by $\hbar$) represent the rate at which an electron placed at the nanowire would leak out through barriers into the electrode and vacuum, respectively. Since $\Gamma_1 \gg \Gamma_2$, $I \approx \frac{2e}{\hbar}\Gamma_2$. On the other hand, the inverse of $\frac{\Gamma_2}{\hbar}$ corresponds to the lifetime τ estimated from the charge leakage rate in the simulation and, as such, $I \approx \frac{2e}{\tau}$, which is the field-emission current that we obtained in the above.

Next, we examine the emission patterns. Figure 3(b) shows the difference in a squared wavefunction between $t = 0$ and $t = 50$ au. The shapes of the emission patterns show that the symmetry in the xy-direction is maintained. Based on the emission patterns, we predict that the projected image of the emission currents for an Ag nanowire will be a nearly circular spot with maximum intensity at the center, because dominant contributions are from the nodeless state.

The magnitudes of the emission currents as a function of increasing electric field are shown in figure 4(a). The emission current increases exponentially with respect to the external electric field, which results in a linear F–N plot in figure 4(b). A comparison with carbon nanotubes is worth mentioning. In the case of carbon nanotubes, localized states are present at the tip region and they were found to be the main sources of the emission currents, in contrast to the nanowire, where the extended states from the s-bands contribute to most of the emission current. Under the same local electric field, which is a condition suitable for comparing FE currents from different systems, the magnitude of the FE current for an Ag nanowire is bigger by one to two orders compared to those of carbon nanotube in pristine [11] or doped [15] conditions. The enhancement of emission current for an Ag nanowire is attributed to the nodeless feature of some states at the Fermi level, as discussed above.

We also calculate FE currents for an ultrathin Au nanowire that has the same atomic structure as an Ag nanowire. The main mechanism of FE is the same as in the case of an

Ag nanowire, i.e. the states near the Fermi energy consist mainly of s-orbitals, and the states without any nodes in the plane perpendicular to the emission direction give the biggest currents. However, the calculated emission current for the Au nanowire under an E_{ext} of 0.3 V Å^{-1} is 0.3 μA, which is only one third of the value for the Ag nanowire, 1.0 μA, calculated under the same conditions. This can be well understood from the work function of the two metals, which are 4.7 and 3.7 eV for Au and Ag, respectively. The higher work function for Au means a larger energy barrier for tunneling to vacuum, which should result in smaller currents.

5. Conclusion

In summary, we have carried out simulations and theoretical analyses of FE for an ultrathin Ag nanowire within the first-principles approach. The distribution of emission currents shows that the states without nodes in the plane perpendicular to the direction of emission give predominantly large currents. For metal nanowires with larger radii, we note that the number of states with nodes would significantly increase. Even though FE currents for those states are relatively small, their total sum could be compatible with or larger than the contribution from a single nodeless state. Therefore, the dominance of the s-like state is likely to persist only for nanowires with a radius of less than 10 nm. The computed FE currents for an ultrathin Ag nanowire are bigger by orders of magnitude than those of carbon nanotubes, and therefore an Ag nanowire is intrinsically a promising FE emitter that can operate under small electric fields. In addition, the chemical inertness of Ag, especially with respect to oxidation, and the extended nature of the emitting states would contribute to stabilizing FE currents under the operation conditions.

Acknowledgments

References

[1] Cui Y, Wei Q, Park H and Lieber C M 2001 *Science* **293** 1289
[2] Yan X-M, Kwon S, Contreras A M, Koebel M M, Bokor J and Somorjai G A 2005 *Catal. Lett.* **105** 127
[3] Beckman R, Johnston-Halperin E, Luo Y, Green J E and Heath J R 2005 *Science* **310** 465
[4] Husain R, Hone J, Postma H W Ch, Huang X M H, Drake T, Barbic M, Scherer A and Roukes M L 2003 *Appl. Phys. Lett.* **83** 1240
[5] Davydov D N, Sattari P A, AlMawlawi D, Osika A and Haslett T L 1999 *J. Appl. Phys.* **86** 3983
[6] Lee C J, Lee T J, Lyu S C, Zhang Y, Ruh H and Lee H J 2002 *Appl. Phys. Lett.* **81** 3648
[7] Ward B L, Nam O-H, Hartman J D, English S L, McCarson B L, Schlsser R, Sitar Z, Davis R F and Nemanich R J 1998 *J. Appl. Phys.* **84** 5238
[8] Lee Y H, Choi C-H, Jang Y T, Kim E-K, Ju B-K, Min N-K and Ahn J-H 2002 *Appl. Phys. Lett.* **81** 745
[9] Zhang G-M, Emmanuel R, Liu H W, Liu W-M, Hou S-M, Kui Y-Z and Xue Z-Q 2002 *Chin. Phys. Lett.* **19** 1016
[10] Fowler R H and Nordheim L 1928 *Proc. R. Soc.* A **119** 173
[11] Han S and Ihm J 2002 *Phys. Rev.* B **66** 241402
[12] Han S, Lee M H and Ihm J 2002 *Phys. Rev.* B **65** 085405
[13] Son Y-W, Oh S, Ihm J and Han S 2005 *Nanotechnology* **16** 125
[14] Tada K and Watanabe K 2002 *Phys. Rev. Lett.* **88** 127601
[15] Ahn H S, Lee K-R, Kim D-Y and Han S 2005 *Appl. Phys. Lett.* **88** 093122
[16] Hong B H, Bae S C, Lee C W, Jeong S and Kim K S 2001 *Science* **294** 348
[17] Sánchenz-Portal D, Ordejón P, Artacho E and Soler J M 1997 *Int. J. Quantum Chem.* **65** 453
[18] Soler J M, Artacho E, Gale J D, García A, Junquera J, Ordejón P and Sánchez-Portal D 2002 *J. Phys.: Condens. Matter* **14** 2745
[19] Ceperley D M and Alder B J 1980 *Phys. Rev. Lett.* **45** 566
[20] Troullier N and Martins J L 1991 *Phys. Rev.* B **43** 1993
[21] Kresse G and Furthmüller J 1996 *Phys. Rev.* B **54** 11169
[22] Suzuki M 1990 *Phys. Lett.* A **146** 319
[23] Sugino O and Miyamoto Y 1999 *Phys. Rev.* B **59** 2579
[24] Datta S 1995 *Electronic Transport in Mesoscopic Systems* (Cambridge: Cambridge University Press)